Electrochemical tools to disclose the electrochemical reduction mechanism of CO_2 in aprotic solvents and ionic liquids

Silvia Mena,[1] Esteve Ribas,[1] Clara Richard,[1] Iluminada Gallardo[1], Jordi Faraudo,[2] Scott K. Shaw,[3,*] and Gonzalo Guirado[1,*]

[1]Departament de Química, Universitat Autònoma de Barcelona (UAB), Campus de la UAB, 08193 Bellaterra, Barcelona, Spain.

[2]Institut de Ciencia de Materials de Barcelona (ICMAB-CSIC), Campus de la UAB, 08193 Bellaterra, Spain.

[3]Department of Chemistry, University of Iowa, Iowa City, Iowa 52242, United States.

e-mail: scott-k-shaw@uiowa.edu ; gonzalo.guirado@uab.cat

ABSTRACT

Carbon dioxide (CO_2) plays a key role in controlling the temperature of the Earth. But the increase in the concentration of CO_2 in the atmosphere brings with it a series of consequences, originating several environmental problems. The use of electrochemical, spectroscopic and molecular dynamics techniques are useful toolkits to valorize carbon dioxide, and to know the reduction mechanism as a function of CO_2 concentration, the cathode nature, and the electrolyte. This manuscript will be mainly centered in the use of ionic liquids (IL) for efficient CO_2 capture and valorization into different valuable products thanks to the CO_2 electrochemical reduction. In this sense, spectroelectrochemistry based on cyclic voltammetry coupled with Polarization Modulation-Infrared Reflection-Absorption Spectroscopy (PM-IRRAS) and Infrared Reflection-Absorption Spectroscopy (IRRAS) appear to be an efficient instrument to follow the CO_2 reactivity in imidazolium ionic liquids. Finally, we present molecular dynamics paired with cyclic voltammetry in order to calculate the diffusion coefficient of CO_2 and the number of electrons involved in its reduction process, respectively. Therefore, the current research opens the door to the use of theoretical-experimental approaches altogether to determine how is the CO_2 reduction mechanism. The CO_2 reduction products in function of the solvent and nature of the cathode is suggested, proving that the product obtained from the electrochemical reduction of CO_2 depends on the electrode material and the solvent.

Keywords: Carbon dioxide, Ionic Liquids, Electrochemistry, Reduction Mechanism.

Graphical Abstract

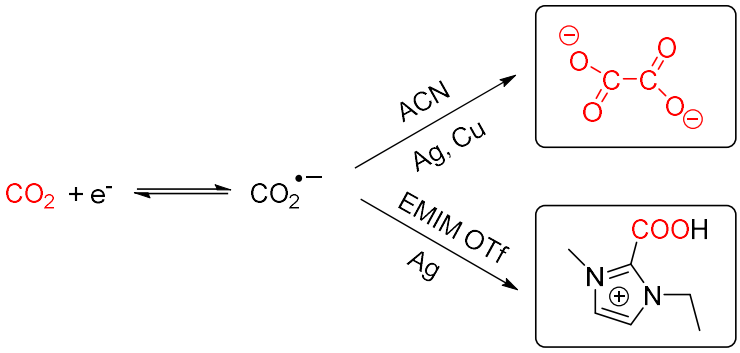

1. INTRODUCTION

Carbon dioxide (CO_2) is possibly the most well-known molecule. It played a vital role in the origin of life[1] and, as it is the main source of energy of plants and some bacteria, is still essential for all living beings on Earth. CO_2 is also one of the main products of the combustion of organic material, such as the widely used fossil fuels. Since the prehistoric era, the humanity has used combustion as a main source of energy and, therefore, it has become the basis of the technological development. In this sense, anthropogenic CO_2 emissions, such as fossil fuel combustion and net land use, have become significantly important since the industrial revolution (since the 1760s). CO_2 concentrations have increased by 40% since pre-industrial times.[2,3] Atmospheric CO_2 is the primary greenhouse gas. An excessive amount of this gas causes an increase in atmospheric temperature which is leading to severe environmental problems.[4] Moreover, predictions suggest that the excessive emission of CO_2 in the atmosphere and the associated global warming will have a negative impact in the global economy.[5,6]

This creates a need to reduce CO_2 emissions by searching alternative sources of energy and diminishing the use of fossil fuels, as well as trying to reduce the CO_2 levels in the atmosphere by directly capturing this molecule. One of the solutions proposed was carbon capture and storage (CCS) strategies,[7] which comprises several processes and materials used in order to retain CO_2, allowing its permanent storage in, for example, underground reservoirs. Furthermore, the carbon capture technologies can be adapted to transform CO_2 into more valuable products.[8] CCS technologies can play a key role in softening the transition into an emission-free society, as can able the use of conventional sources of energy, reducing the emitted CO_2. Nowadays, postcombustion carbon capture systems are the most mature technology and the easiest to adapt, as they can be directly used in current power plants or other sources of CO_2.[9] Moreover, these technologies can be extremely helpful in reducing the emissions in other sectors which are difficult to decarbonize.

Amine scrubbing processes are the most used mechanisms for postcombustion CO_2 capture.[10] In this process, mixing of gaseous CO_2 molecules takes place in an absorbent liquid solvent which is lately regenerated. Chemical absorption by aqueous amine-based solvents appears the most promising near-term solution for CO_2 capture from flue gas, because of their ability to capture CO_2 at low pressure with adequate absorption/desorption kinetics. CO_2 removal from flue gases is practiced on a large scale using aqueous solution of amines such as monoethanolamine (MEA) and diethanolamine (DEA), which have more than 90% of efficiency.[11] To liberate the CO_2 at a higher concentration, these amine solutions are then regenerated by steam stripping. These liquid solvent-based technologies for carbon capture present several

drawbacks like amine loss in the regeneration process, after the capture of the CO_2, or degradation of the solvent due other chemicals found in flue gases.[12]

For this reason, searching alternatives to amines as absorbents has grown enormously in recent years. One of the most fertile research fields on this process has been the ionic liquids (IL), because they are capable to overcome this kind of problems.[13–15] Unlike MOFs, which are frequently considered in CCS systems,[16] IL degrade at temperatures over 300 ºC and are, typically, non-flammable. Stability vs elevated temperatures and non-flammability are important in CCS applications to improve safety and to allow a greater lifespan, reducing costs.[7,17,18] ILs are constituted purely by the combination of anions and cations, which are typically bulky and asymmetric to hinder crystalization.[7] Due to their inherent advantages (melting point below 100 ºC), IL are often considered as a solvent in CO_2 valorization processes, which consists in the transformation of captured CO_2 in other valuable products. In this sense, the use of electrochemical approaches to transform waste CO_2 into valuable chemical products in one of the most studied processes to valorize CO_2. ILs also offer wide electrochemical windows, which enhances the tunability of electrochemical reactions.[18–21]

Selecting the adequate reagents, different molecules of interest can be synthetized by an electrocarboxylation process, i.e., fixing the CO_2 electrochemically to form a carboxylic acid.[22–29] Examples of molecules that can be synthetized following this process are non-steroidal anti-inflammatory drugs (NSAID), such as ibuprofen and naproxen.[30,31] These molecules are valuable pharmaceutical products that, thanks to the use of IL, can be obtained by green synthesis processes.[32,33]

Considering previous works on aprotic solvents, there are two main pathways of reaction that follow diverge after CO_2 is reduced into its radical anion specie (reaction 0, scheme 1). In one of these pathways the reaction follows the formation of oxalate ($C_2O_4^{2-}$), from the dimerization of two $CO_2^{\cdot-}$ radicals, which involves only one electron transfer (reaction 1). The other pathway (reaction 2) involves the formation of an radical anion intermediate trough the reaction between $CO_2^{\cdot-}$ and a molecule of CO_2, which evolve into carbonate (CO_3^{2-}), carbon monoxide (CO) and carbon dioxide (CO_2), reactions 3 and 3'. In this second pathway, the electrochemical reduction mechanism of CO_2 involves two electrons.[34]

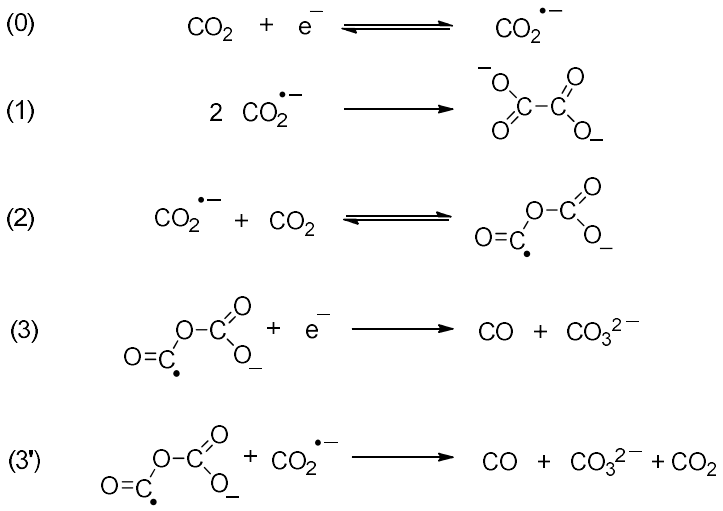

Scheme 1. CO_2 reduction reaction and products formation in aprotic solvents adapted from reference 34.

The solvent and the electrode employed for reducing the captured CO_2 can affect what product, is synthetized and the process efficiency.[23] For this reason, the aim of this work focuses on introducing different approaches in order to disclose the CO_2 electroreduction mechanism. Determining the number of electrons involved in the reduction process is a crucial parameter that gives information about how the reaction takes place. Thanks to the information given by cyclic voltammetry and molecular dynamics simulations, we can quickly determine this parameter and predict if the chosen electrode material and solvent are suitable for obtaining desired CO_2 electroreduced products.

2. MATERIALS AND METHODS

2.1. Materials

Carbon dioxide (CO_2) and nitrogen (N_2) were purchased from Carburos Metálicos S.A. (Cornellà de Llobregat, Spain), purity of 99.9999%). All the commercially available reagents, acetonitrile (ACN) and tetrabutylammonium tetrafluoroborate ($TBABF_4$) were acquired from Sigma-Aldrich (Madrid, Spain) with maximum purity and used as received. Titanocene was received from AFINITICA and used without further purification. 1-Ethyl-3-methylimidazolium bis(trifluoromethylsulfonyl)imide (EMIM TFSI) was acquired from Solvionic (Toulouse, France) and were dried with activated molecular sieves for 24 h in order to guarantee that the amount of water was always less than 100 ppm.

1-Ethyl-3-methylimidazolium trifluoromethanesulfonate (EMIM OTf) was synthesized following the procedure described in Scheme 2. In a three-neck 500 mL flask, 50 g of methyl trifluoromethanesulfonate was dissolved in benzene and was slowly mixed with 28 g of 1-ethylimidazole, which was solved previously in benzene keeping the temperature at 0 ºC. After the reaction was finished, the solvent was removed, and the crude was purified under vacuum using activated carbon. The final IL was characterized by ^{1}H-NMR (400 MHz, D_2O) and Karl Fischer. Prior to use, the ILs was dried under vacuum to remove traces of water and was stored under ultrapure dinitrogen (Praxair, Inc., Danbury, CT, U.S.A.) in a nitrogen glovebox with <10 ppm of water. Water content analysis of ILs was carried out on an 831 Karl Fischer (KF) coulometer (Metrohm, Riverview, FL, U.S.A.).

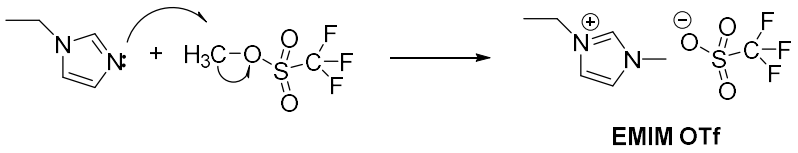

Scheme 2. Synthesis of EMIM OTf.

2.2. METHODS

The theoretical-experimental approach described is divided in two parts. Firstly, molecular dynamics (MD) are employed to determine the diffusion coefficient of the CO_2 in EMIM TFSI. Secondly, electrochemical techniques are used to obtain the number of electrons involved and disclosed the CO_2 electroreduction mechanism in imidazolium ionic liquids.

2.2.1. Molecular Dynamics simulations of CO_2 diffusion in EMIM TFSI

All atomic Molecular Dynamics simulations were employed in order to determine the diffusion coefficient of a CO_2 molecule in the IL of interest. In our simulations, we considered the motion of a single CO_2 molecule inside an IL made by 499 EMIM TFSI pairs at T= 298 K and 1 atm of pressure. The resulting system with a single CO_2 molecule and 499 EMIM-TFSI pairs (a total of 16969 atoms) is shown in Figure 1. As only one CO_2 molecule is included inside the IL liquid box composed by 499 pairs, hence the simulated CO_2 concentration is 7.69 mM. This value is obtained considering a single molecule of CO_2 within a simulation box volume of 216000 Å3 (60 x 60 x 60 Å). The interactions between atoms during the simulation were modelled using previously developed forcefields. The employed forcefield for the IL was the nonpolarizable forcefield previously developed by Brela et al.[35] for NAMD simulations of EMIM TFSI. This forcefield has been validated by comparing with Ab Initio MD simulations (it correctly reproduces correlation functions and spatial distributions of donor-acceptor pairs in EMIM TFSI) and it also correctly predicts observables such as the experimental density of the IL (predicted value 1.515 g/cm^3, experimental value 1.518 g/cm^3). The CO_2 molecule was described using the CHARMM36 general force field[36] as in our previous work on simulations of liquid solutions containing CO_2.[36] The simulations were performed using Nanoscale Molecular Dynamics (NAMD) 2.13 program[37] and the visualization and analysis of the results was performed using the Visual Molecular Dynamics (VMD) program[38] and our own scripts. In our simulations, the equations of motion for all the atoms were solved with a time step of 2 fs. Temperature and pressure were kept constant at 298 K and 1 atm using a Langevin thermostat (relaxation time 1 ps) and the isotropic Nosé-Hoover-Langevin piston (oscillation period of 100 fs and decay time of 50 fs). Electrostatic interactions were computed using the PME method (PME) with the standard settings in NAMD (1 Å resolution, updated each 2 times steps). Lennard-Jones interactions were truncated at 1.2 nm employing a switching function starting at 1.0 nm. Periodic boundary conditions were employed in all directions.

The protocol followed in the simulations was the following. First, we randomly inserted a CO_2 molecule inside a pre-equilibrated IL originally made by 500 EMIM TFSI pairs (the pre-equilibrated liquid coordinates were kindly provided by the authors[35]). An EMIM molecule was deleted due to overlap with

the randomly inserted CO_2 molecule and a random nearby TFSI molecule was deleted in order to preserve electroneutrality. Before production, the system required further equilibration due to this deletion/insertion process was energy minimized and equilibrated for ~1 ns until we observed full equilibration of the thermodynamic magnitudes (temperature, pressure, energy and volume of the system). After equilibration, we performed a full production run of 400 ns, monitoring the trajectory of the CO_2 molecule. This long simulation time was selected not only to ensure that the CO_2 molecule is able to explore the IL away from its initial neighbors but also to ensure equilibration of the IL which is a liquid with sluggish dynamics, as seen previous simulations.[35] The motion of the CO_2 molecule inside the IL was analyzed and the diffusion coefficient was extracted, as discussed in the Results section.

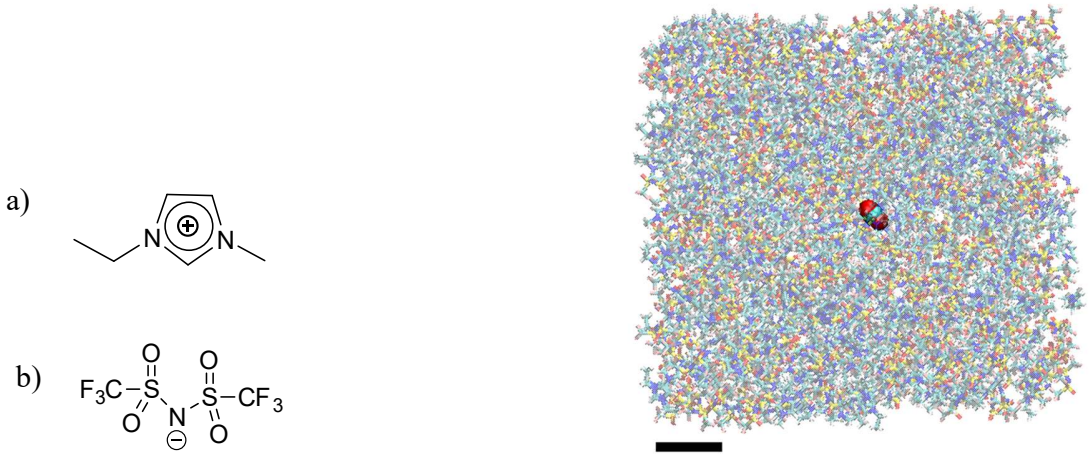

Figure 1. Left; Molecular structure of EMIM(a) and TFSI (b). Right: Snapshot of the initial configuration for a CO_2 molecule inside an EMIM-TFSI liquid box considered (scale bar = 1 nm). The CO_2 molecule was shown in Van der Waals representation and the EMIM TFSI ions were shown as transparent bonds to facilitate visualization. The employed color code was CPK (O:red, N:blue, C:cyan, S:yellow, F: pink).

2.2.2. Electrochemical Experiments

An electrochemical conical cell was used for the set-up of the three-electrode system. For cyclic voltammetry (CV) experiments of aprotic solvents and EMIM TFSI, the working electrode were a silver disk and copper disk, both with a diameter of 1.6 mm and a glassy carbon disk with a diameter of 1 mm. They were polished using a 1 mm diamond paste. The counter electrode was a Pt disk < 1 mm in diameter. All the potentials were reported versus an aqueous saturated calomel electrode (SCE) isolated from the working electrode compartment by a salt bridge. The salt solution of the reference calomel electrode was separated from the electrochemical solution by a salt bridge ended with a frit, which was made of a ceramic material, allowing ionic conduction between the two solutions and avoiding

appreciable contamination. Ideally, the electrolyte solution present in the bridge is the same as the one used for the electrochemical solution, in order to minimize junction potentials. The error associated with the potential values was less than 5 mV. The ohmic drop can be one of the main sources of error when IL are used as solvents, since they are more resistive media than polar aprotic solvents with 0.10 M concentration of supporting electrolytes.

In the case of EMIM OTf All electrochemical experiments were carried out with a CHI 660D electrochemical analyzer (CH Instruments, Austin, TX, U.S.A.), at room temperature and ambient pressure. For working electrode, disk-shaped substrates to support IL films are cut from 14 mm-diameter polycrystalline silver rods (99.99% purity, ESPI Metals, Portland, OR). The disk surfaces are mechanically polished to 0.3 μm grit size with alumina powder to obtain a mirror finish. Subsequent chemical polishing uses a well-established method including an acid etch, which employs H_2SO_4 (ACS grade, BDH), $HClO_4$ (70%, Sigma), and NH_4OH (28−30%, BDH), all used as received, along with an aqueous solution of 4 M CrO_3 (99.9%, Aldrich) and 0.6 M HCl (ACS grade, BDH). All solutions are prepared with ultrapure water (18.2 MΩ cm^{-1} with TOC ≤ 4 ppb) generated by a Milli-Q UV Plus System (Millipore Corp). Two different Pt wires (99.997% metal basis, Alfa Aesar) serve as the quasi-reference and auxiliary electrodes, respectively.

Infrared reflection *absorption spectroscopy (IRRAS)*; IR radiation from the Fourier Transform Infrared Spectroscopy (FTIR) spectrometer source is passed through a wire grid polarizer to create a p-polarized beam, which is impinged on the surface at a glancing angle of ca. 78° from the normal. This arrangement is made on an external optical bench in a custom enclosure purged with dry, CO_2-free air. Background spectra are collected in the same geometry using a freshly polished, cleaned, and dry substrate. The combination of incident p-polarized light and selection rules of IRRAS on metal substrates allow absorption by any molecular vibrations with a component of their dipole moment perpendicular to the Ag surface. All IRRAS spectra are averaged over 1000 scans.

Polarization *Modulation-Infrared Reflection-Absorption Spectroscopy (PM-IRRAS);* Its measurements were carried out using a Thermo-Nicolet iS50 Fourier transform spectrometer with an external bench utilizing a photoelastic modulator (PEM) from HINDS Instruments and a GWC Instruments demodulator. A liquid nitrogen-cooled MCT-A detector was used for all IR measurements. The IR beam was p-polarized using a wire grid and passed through the PEM before being focused onto the top portion of the substrate at an angle of 78 ± 3° with respect to the surface normal. Each spectrum was averaged over 1000 scans and recorded with 4 cm^{-1} resolution.

For both spectroscopy techniques it was important to have the cell completely closed for maintaining the desired atmosphere (Figure 2).

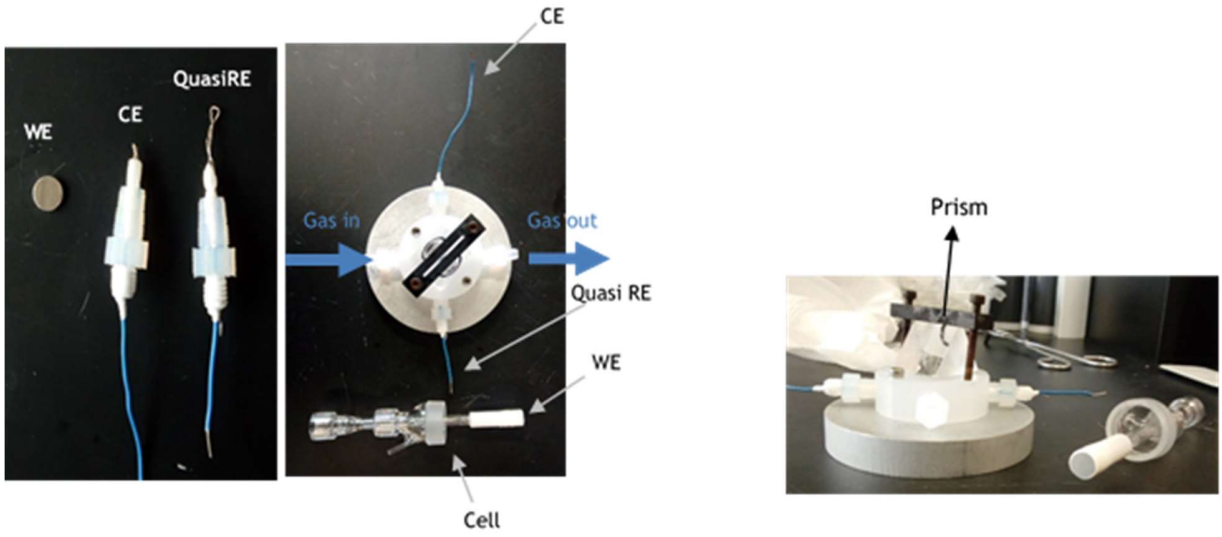

Figure 2. a) Three electrode system: Ag WE, Pt CE, Pt QuasiRE. b) Spectroelectrochemistry cell disposition with the prism which allows to change IR beam direction.

2.2.3. Determination of the CO_2 concentration in the electrolytic media

A thermal mass flow meter of modular construction with a 'laboratory style' pc-board housing (EL-FLOW® Mass Flow Meter/Controller, Bronkhorst Hi-Tec, Ruurlo, Netherlands) was used to monitor the CO_2 concentrations in the solution. Control valves are integrated to measure and control a gas flow from the lowest range of 0.2–10 mL/min. To calculate the CO_2 concentration in the solvent, we have considered the bubbling conditions (time, flow rate, density, and temperature) to quantify the amount of CO_2 introduced, the purity of CO_2, and the volume of the solution. Average data is shown for 3 independent measurements in pure solvents. Secondary methods have been used for verifying the CO_2 concentration values. In this sense, Titanocene (E^0= -1.07 V vs SCE) was used as a one-electron redox probe in ACN. A closer look at the CVs revealed that the peak currents are of the same order of magnitude as expected for one electron transfer reactions of a diffusing solution species in ACN using the same experimental set-up. Finally, a gravimetric methodology [18] was used as a non-electrochemical secondary for validating CO_2 concentrations in ionic liquids.

3. RESULTS AND DISCUSSION

3.1. Electrochemical reduction mechanism of CO_2

This section establishes the electrochemical reduction mechanism of CO_2 in aprotic electrolytes (stating from organic aprotic solvents and moving to imidazolium ionic liquids) using different cathode materials (carbon, silver and copper). We analyze CO_2 saturated-acetonitrile solutions with different working electrodes (specially Cu, Ag and GC) to determine whether the electrochemical methods employed are reliable and useful to achieve a good understanding of the CO_2 behavior in those system. We compare these results to those in imidazolium IL solvent (EMIM TFSI) so as to determine the influence of the solvent in the CO_2 reduction products.

3.2.1. Electroreduction mechanism of CO_2 in acetonitrile using different cathodes

In order to analyze the reduction reaction mechanism of CO_2, several cyclic voltammograms are done in the electrolytic media for varying concentrations of CO_2, across three electrode materials (Figure 3a-c). As a result, a new reduction peak that increases when the amount of CO_2 in solution is growing. This reduction peak appears at -2.3V vs and at -2.5 V vs SCE when silver or copper are used as a cathode, respectively (Figure 3a-b). This first electrochemical process is related to the reduction of CO_2 to its radical anion in the working electrode surface. The shape of the CO_2 reduction peak is related with the peak splitting (ΔE_p), which is determined difference between the cathodic peak potential (E_{pc}) and the half-peak potential (where the $I_{pc} = I_{pc/2}$).[39] In both cases, the ΔE_p value is 118 mV, which indicates a slow electron transfer process. Finally, in the case of using GC as a cathodic material, the reduction feature is not observed, hence it was decided to discard this electrode for further experiments.

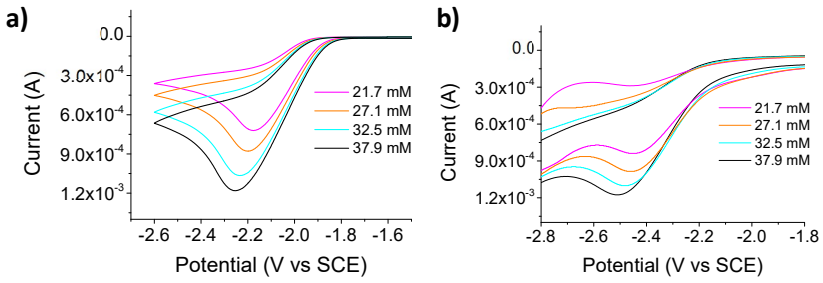

Figure 3. CV for different concentrations of CO_2 in the ACN + 0.10 M $TBABF_4$ solution. Scan rate (ν) of 0.5 V/s. T = 25 ºC. Pt CE, SCE RE, Working electrode **(a)** Ag (d = 1.6 mm) **(b)** Cu (d = 1.6 mm)

Figures 4 represents observed peak currents versus the amount of CO_2 in the solution, recorded for silver and copper electrodes. Current saturation is observable as the concentration of CO_2 in the solution increases beyond ca. 250 mM for Ag and ca. 150 mM for Cu.

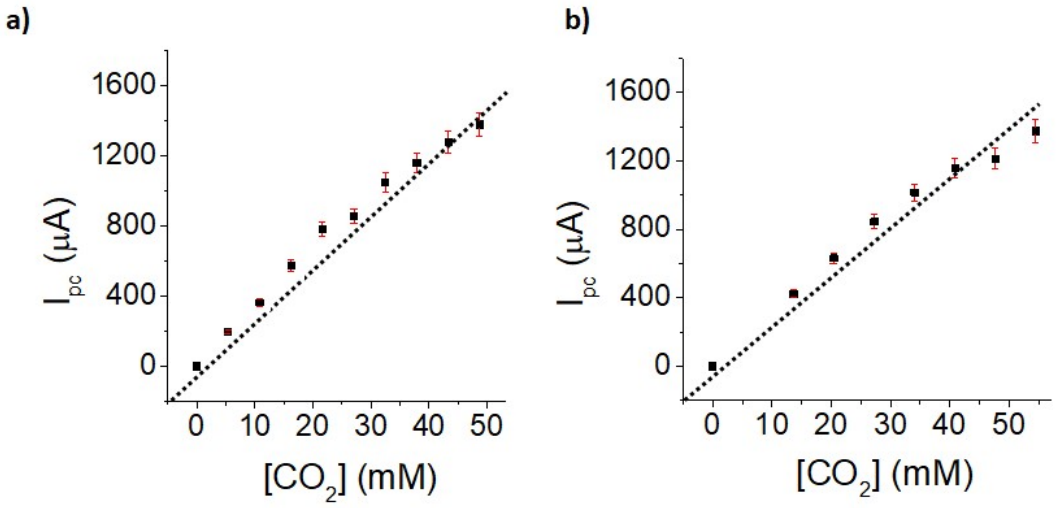

Figure 4. Current peak for the cathodic process, i_{pc}, versus the CO_2 concentration, $[CO_2]$. Working electrode **(a)** silver (d= 1.6 mm) **(b)** copper (d= 1.6 mm). Pt CE. SCE RE. The I_{pc} differences depicted in Figure 4 are the averages of three independent determinations.

The saturation values are useful to determine the activity of electroactive species in the solution. However, with the aim of calculating the number of electrons involved in the reduction, we focus on the linear part of the plot which and apply the Randles-Sevcik equation.[40] It is important to highlight that from the voltammograms observed in figure 3, the reduction process of CO_2 in acetonitrile is clearly non-reversible, as no anodic peak is observed. Therefore, the equation is adapted in order to describe the process observed in this case (Equation 1):[41]

$$i_{pc} = (2{,}98 \cdot 10^5)\, A\, n^{\frac{3}{2}}\, D_i^{\frac{1}{2}}\, v^{\frac{1}{2}}\, c_i\, \alpha^{\frac{1}{2}} \qquad (1)$$

The Faraday constant and the temperature are grouped into the numeric constant displayed in the equation. The other parameters refer to *A*, area of the working electrode; *n*, is the number of electrons involved in the process, *D*, is the diffusion coefficient of CO_2 in the solvent considered;[42] *v*, is the scan rate of the cyclic voltammetry; c_i is the bulk concentration of the electroactive specie of interest (CO_2) in the solvent; finally, the charge transfer coefficient (α), which can be calculated from the peak with value (ΔEp),[40] is 0,4 for both electrodes. The α value only appears in equation 1 since the rate

of the electron transfer is slow. Values of α smaller than 0.5 are in good agreement with decreasing rate constant values.

As a result, the number of electrons (*n*) involved in the CO_2 reduction reaction determined from the slope (Figure 4) in acetonitrile, using the working electrode of silver and copper are 1.1±0.3 and 0.85±0.3, respectively. These results are in good agreement with the fact that the electrochemical reduction mechanism of CO_2 in acetonitrile is a dimerization process leading to the formation of oxalate as a final product.

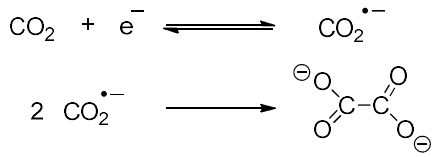

Scheme 3. Reduction of CO_2 in acetonitrile, an aprotic solvent with Ag and Cu working electrodes.

3.2.2. Disclosure of the electroreduction mechanism of CO_2 in EMIM TFSI using altogether Cyclic Voltammetry and Molecular Dynamics simulations

The behavior of the CO_2 in the ionic liquid EMIM TFSI is analyzed using cyclic voltammetry in order to study the influence of the electrolyte in its reduction mechanism. Figure 5 displays the voltammograms for a saturated-CO_2 solution (0.4 M [CO_2], determined through thermal mass flow-meter which monitored a gas flow of 10 mL/min) in EMIM TFSI (in red) and the same solution at inert atmosphere, N_2, (in black), using silver and copper as working electrodes (Figure 5a and 5b, respectively). CV response shows an irreversible slow electron transfer at -2.05 V vs SCE with silver working electrode and at -2.45 V vs SCE with copper working electrode. It is also observed that rate of the electron transfer is electron transfer with copper electrode is slower than silver working electrode, showing an α value of 0.18 (Cu) and 0.33 (Ag) calculated with value (ΔEp),[40]·[43] respectively.

Before determining the number of electrons involved in this first reaction, it is needed to calculate the diffusion coefficient of CO_2 in this solvent. Although, different methodologies have been previously applied for determining (D_{CO2}),[44,45] in the current work we decide to use molecular dynamics (MD) simulations, which is an essential technique to study a variety of molecular properties including molecular diffusion. Employing molecular dynamics (MD) simulations for calculating diffusion coefficients is an appealing alternative to the experimental approaches, which very often include high cost or technical difficulties when high pressures and/or temperatures are involved.[44] Hence, in the current section it will be combined molecular electrochemistry and molecular dynamics tools for a first time.

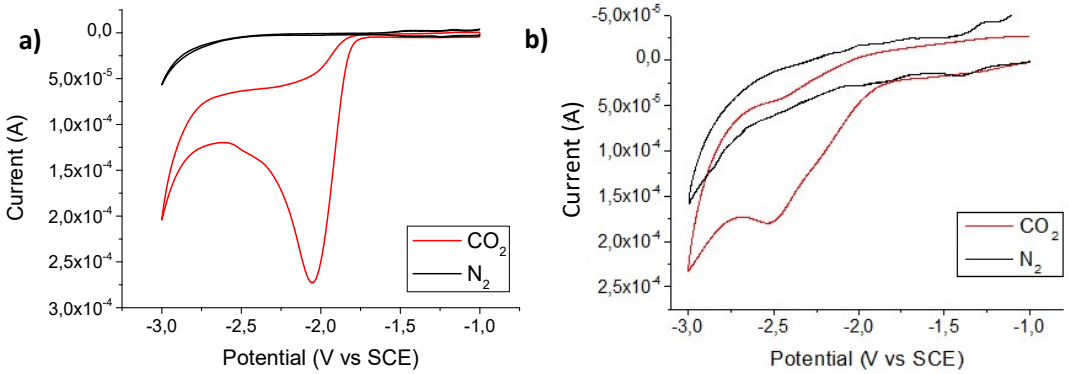

Figure 5. Voltammogram for solutions of EMIM TFSI with 0.45 M CO_2 (red) and N_2 (black). Scan rate: ν = 0.5 V/s. T = 25 ºC. Pt CE, SCE RE, Working electrode **(a)** silver (d = 1.6 mm) **(b)** copper (d = 1.6 mm).

Determination of diffusion coefficient of CO_2 in EMIM TFSI from MD simulations

A simulation of a time interval of 1 ns was run, after the equilibration process, obtaining the position of the CO_2 versus time. We have analyzed both qualitatively (trajectory visualization) and quantitatively (diffusion coefficient) the motion of a CO_2 molecule inside an EMIM TFSI liquid at 298K and 1 atm using molecular dynamics simulations (see Methods). The motion of the molecule during a short fragment of the trajectory (1 ns) is illustrated in Figures 6 and 7. As seen in these figures, the motion of the CO_2 molecule has the typical appearance of a Brownian motion, moving faster than neighboring IL molecules, as should be expected. As seen in Figure 6, the displacement of the CO_2 molecule inside the simulation box during 1 ns is substantial. It should be noted that during the full 400 ns simulation, the molecule is able to explore the full simulation box, so that significant statistics of the motion of the CO_2 molecule can be collected.

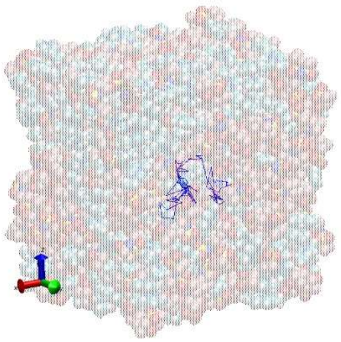

Figure 6. Illustration of the trajectory of the CO_2 molecule inside the EMIM-TFSI liquid during a short fragment of the simulation (1 ns). The initial positions of the atoms from EMIM and TFSI molecules are shown as translucid

spheres with their Van der Waals size. The trajectory of the C atom of CO_2 molecule during 1 ns (with a 10 ps resolution) is shown in blue.

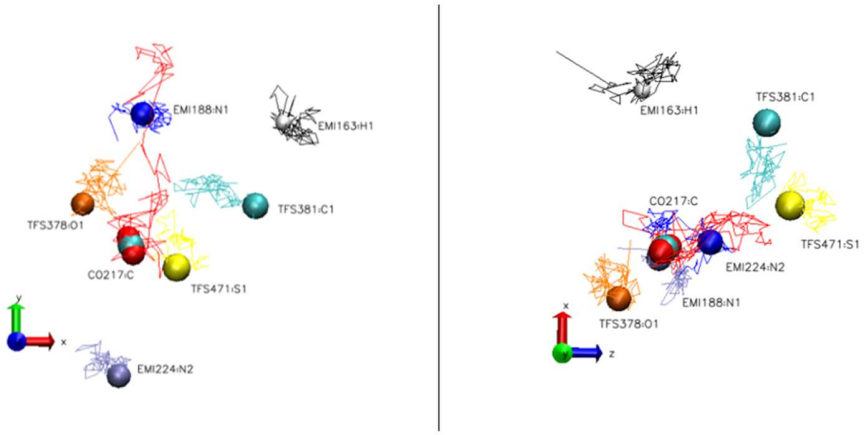

Figure 7. Comparison of trajectories of the CO_2 and IL ions during a 1 ns fragment of the simulations. We show the trajectory of CO_2 molecule (with the structure of the molecule superimposed) as seen in the XY and XZ planes (left and right, respectively, as indicated by the axis). For comparison, we also show the trajectory of some selected atoms from EMIM or TFSI ions located nearby (the label indicates whether the atom corresponds to EMIM or TFSI, the chemical element and a number code identifying each particular atom, the different color for each atom is selected to facilitate visualization).

Quantitatively, the Brownian motion of a molecule is characterized by a motion with zero mean (no average motion over time) but with a mean square displacement (MSD) that grows linearly with time with a slope determined by the diffusion coefficient *D*, according to Einstein relation.[46] In our simulations, the MSD and diffusion coefficient in a particular direction (say for example, the *x* axis) are given by:

$$MSD = \langle |x(t) - \mathrm{x}(0)|^2 \rangle = \sum_{t_0} \frac{1}{N_{t_0}} |x(t + t_0) - x(t_0)|^2 \qquad (2)$$

$$MSD = 2\,D\,t \qquad (3)$$

where x(t) is the x coordinate of a reference atom (in this case, the C atom of CO_2) at time t and and D is the diffusion coefficient (in Eq.(2), the trajectory is sampled over all possible reference times t_0 so that $t+t_0$ is smaller than the final simulation time. Analogous expressions can be written for the motion in all directions (the y and z directions). Using Eq. (2) and (3), the diffusion coefficient of the CO_2 can be obtained from the slope of an MSD vs Time graph (Figure 7). The diffusion coefficient as estimated from the three axes give different values although of the same order of magnitude. This probably reflects the structural complexity of the IL at the molecular level at it may indicate a tendency of the CO_2 molecule to experience an anisotropic diffusion. As a characteristic value of the diffusion coefficient of CO_2 in EMIM TFSI we can take the value obtained for the case for the slowest motion, so we take $D \approx 4 \cdot 10^{-10}$ m^2/s. It is important

to note that the obtained diffusion coefficient and the experimental reference value[41] previously reported are in good agreement considering the methods employed in this work. The number of electrons in the CO_2 electron transfer is determined via equation 1, where the kinetic and thermodynamic parameters required are obtained by cyclic voltammogram and molecular modelling tools, respectively. The number of electrons involved in both instances is rounded to 1. This indicates that the electroreduction of CO_2 in EMIM TFSI is a monoelectronic process. However, after a controlled potential electrolysis process, the electroreduction of CO_2 in these IL does not lead to oxalate as a main product as in the previous section where ACN is used.[41] It is fair to think that in this case a switching in the reaction course of CO_2 is seen in both electrodes after the electrochemical reduction of CO_2. These results seems to be in good agreement with the previously publishes by Kamat and Brennecke[26] for the electrochemical reduction of CO_2 in the same ionic liquid using Pb instead of Ag or Cu as a cathode. In this work, the authors proposed a catalytic role of the ionic liquid. This phenomenon is also observed in our case where the reduction peak potential values are shifted to less negative potential when the ACN is replaced by EMIMTFSI with silver (c.a. ~0.30 V) and copper (c.a. ~0.15 V) cathodes. The CO_2 anion radical is stabilized by the imidazolium IL, which avoids the radical anion dimerization process,[34] and favors on the one hand the production of CO, and on the other hand a carboxylation process where it is obtained an imidazolium carboxylated complex. Note that in both processes the number of electrons involved will be one. At this point, in order to determine if this reaction pathway for the electrochemical reduction of CO_2 is a general mechanism where imidazolium ILs are used, we decided to study the electrochemical process in EMIM OTf instead of EMIM TFSI. This study was performed by terms of spectroelectrochemistry based on cyclic voltammetry coupled with Polarization Modulation-Infrared Reflection-Absorption Spectroscopy (PM-IRRAS) and Infrared Reflection-Absorption Spectroscopy (IRRAS) using silver as a cathode, since the electrocatalytic effect is higher Ag than in Cu cathodes.

3.2.3. Electroreduction mechanism of CO_2 in EMIM OTf using silver as a cathode

A study of the direct reduction of CO_2 at silver surface and EMIM OTf with spectroelectrochemistry based on IRRAS and PM-IRRAS spectroscopy, cyclic voltammetry, and amperometry determinations is performed in order to fully disclose the electrochemical reduction mechanism. The experiments were carried out in three different atmospheres (N_2, CO and CO_2). To have a background and know which frequencies are related to the functional groups, the ionic liquid was characterized in inert atmosphere, with N_2, and carbon monoxide, CO, to have a pattern to compare the products that appear on the spectra in the CO_2 reduction.

EMIM OTf characterization under N_2 atmosphere

Figure 8 shows the cyclic voltammetry response for EMIM OTf, which is reduced at E_{pc} = -2.0 V (vs Pt), due to its imidazolium ring.[47,48]

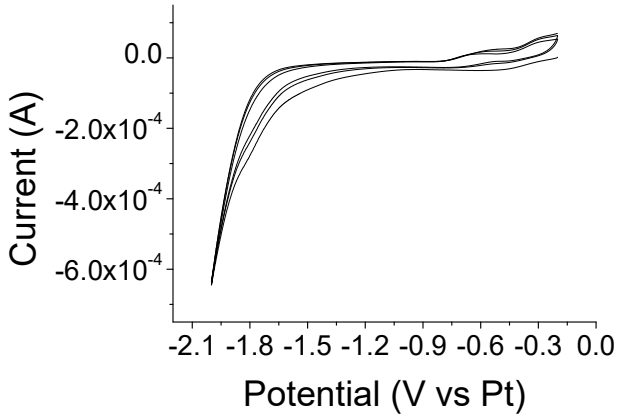

Figure 8. Cyclic voltammetry of EMIM OTf with Ag WE (d = 14mm), Pt CE and Pt QuasiRE. Scan rate (v): 0.5 $V \cdot s^{-1}$. Under N_2 atmosphere. T= 15 ºC.

IRRAS and PM IRRAS spectra (Figure 9) show absorption patterns consistent with functional groups in the ionic liquid. The IRRAS spectroscopy also shows ionic liquid functional groups and the characteristic signatures of environmental water and carbon dioxide vapor. PM IRRAS shows an improvement in the spectra quality by removing the interactions of gas phase water and CO_2, allowing assignment of peaks arising from C=C stretching, C-H bending, and C-N ring stretching vibrations in the cation structure of EMIM OTf.[49,50] The spectroscopic data related to the functional groups of EMIM OTf are summarized in Table 1.

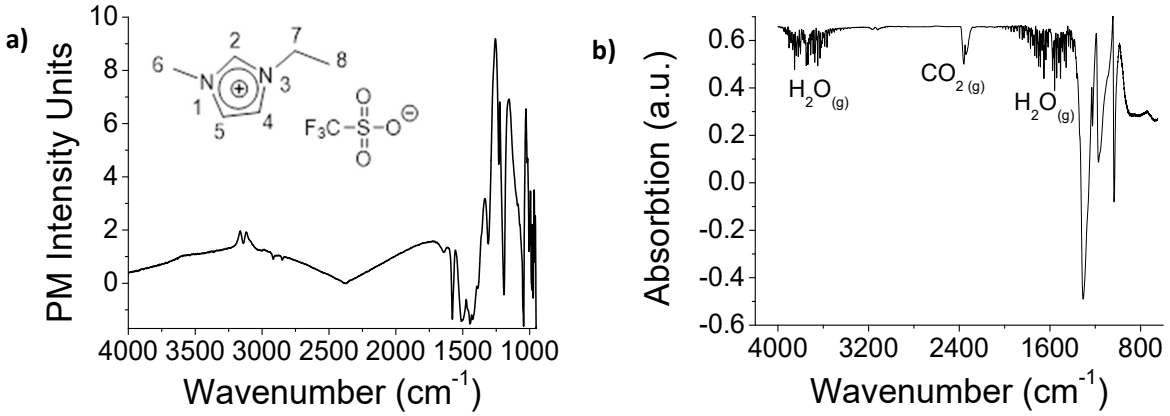

Figure 9. Spectroscopy of EMIM OTf under inert atmosphere on a silver surface **(a)** PM IRRAS spectra **(b)** IRRAS spectra.

Table 1. EMIM OTf spectroscopy characterization.		
Assignments	**IRRAS (cm^{-1})**	**PM IRRAS (cm^{-1})**
SO_3 asym str	1263, 1270	1263, 1270
CF_3 sym str	1226	1226
CF_3 asym str	1165	1165
SO_3 sym str	1032	1032
C(4/5)-H str	3163	3163
C(2)-H str	3120	3120
CH_3 asym str	2990	2990
CH_2 asym str	2956	2956
CH_3 sym str	2890	2890
C=C str / C-N str / C-H b	-	1300-1600

To determine how the ionic liquid is reorganized when applying negative potentials, four different potentials were applied across the electrochemical window of the ionic liquid. The imidazolium ring (1600 – 1300 cm^{-1}) modes increase with more negative potentials (Figure 10). It is concluded from these data, that the cationic part of EMIM OTf would move nearer to the electrode surface as the potential becomes more negative.

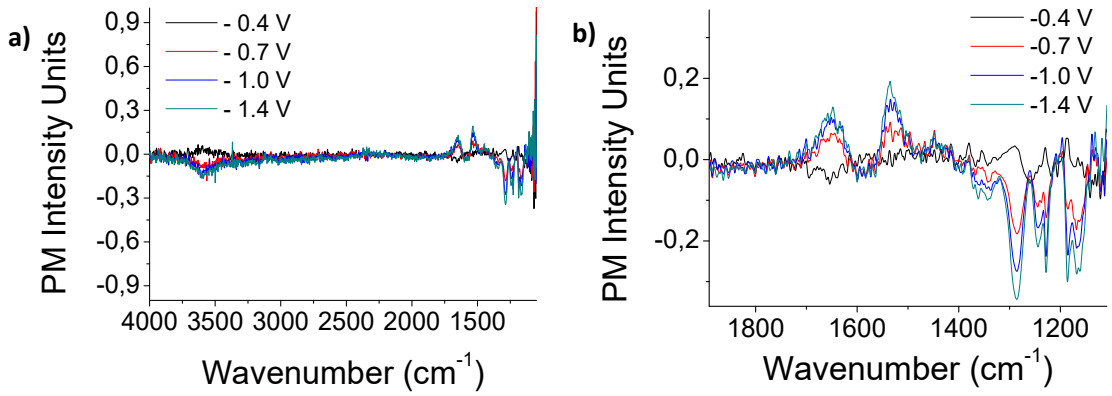

Figure 10. PM IRRAS of EMIM OTf at different applied potentials, after subtraction of blanks, under inert atmosphere. (a) all wavelength (b) zoom at determined wavelength (1100-1900 cm^{-1}).

EMIM OTf characterization under CO and CO_2 atmospheres

Figure 11a shows the cyclic voltammetry response and Figure 11b the IRRAS spectroscopy of the ionic liquid in the three different atmospheres; when the solution was saturated with CO or CO_2, IRRAS spectra changed and new peaks appear at frequencies related to CO (2143 cm^{-1}) or CO_2 (2235 cm^{-1}),

indicating that CO or CO_2 is present in the solution. However, PM IRRAS spectra is the same as inert

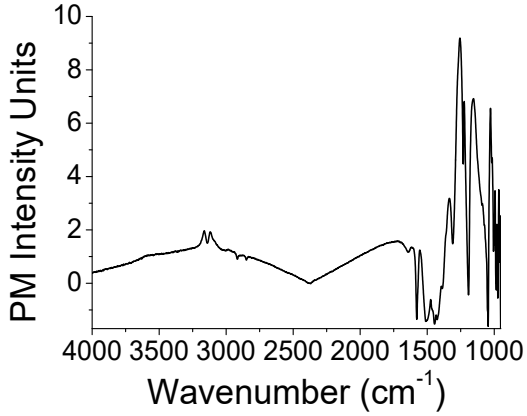

atmosphere (

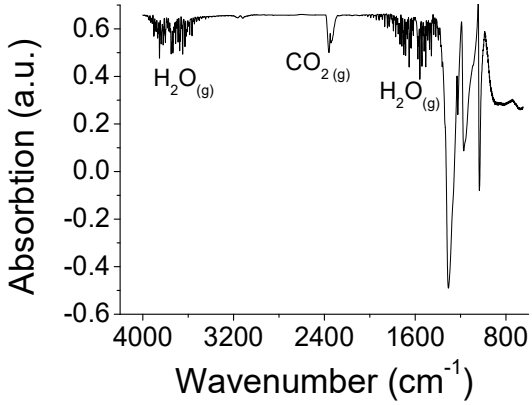

Figure 9a), because this method is 'surface sensitive' and only shows what is happening at the electrode surface. Therefore, just bubbling the gas into the solution of ionic liquid was not enough to show the presence of CO or CO_2 at the working electrode surface.

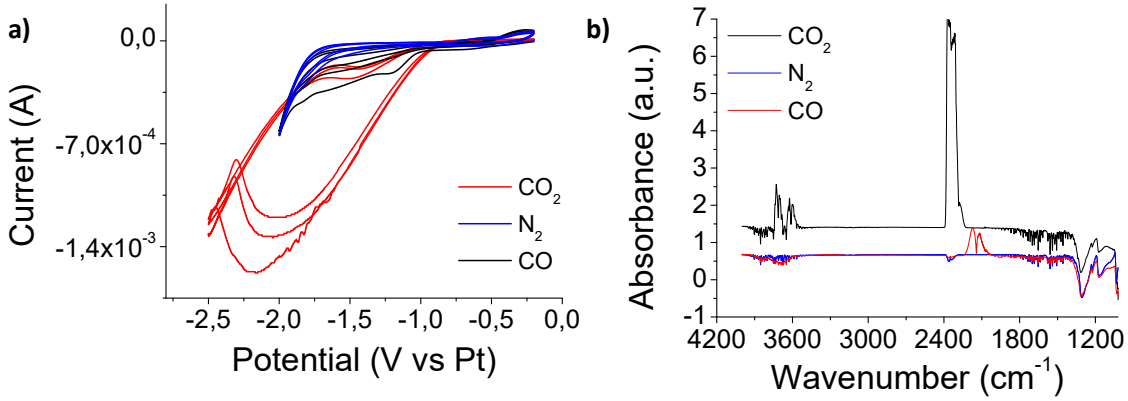

Figure 11. Characterization of EMIM OTf ionic liquid under N_2 (blue line), CO (black line) CO_2 (red line) saturated atmospheres by **(a)** Cyclic voltammetry. Ag (d = 14mm) WE, Pt CE, Pt QuasiRE. T = 15ºC. Scan rate: 0.5 $V \cdot s^{-1}$ **(b)** IRRAS spectroscopy.

Cyclic voltammetry shows a huge peak related to the reduction of CO_2 on the silver surface. But under CO and N_2 atmospheres CV response is not shown, because there was no reduction feature present in the electrochemical potential window of EMIM OTf. To determine what is happening in the ionic liquid and on surface of the working electrode when CO_2 is reduced, different determinations of PM IRRAS were performed, coupled to amperometric determinations at E_{pc} = - 1.5 V, -1.8 V and -2.0 V (vs Pt) in a carbon dioxide saturated atmosphere. Figure 12 shows PM IRRAS spectra of the different applied potentials after 1 h. No change in the structure of the ionic liquid is initially observed, but when the negative potential is applied, the peaks related to cationic part of ionic liquid increase in intensity, which means that imidazolium ring is oriented towards the silver surface.

New peaks (1577 cm^{-1}, 1508 cm^{-1} and 1477 cm^{-1}) also appeared and increased in intensity with potential applied (Figure 12b). These new peaks could be related to a carboxylated species on the structure of the ionic liquid, because when the ionic liquid was characterized under inert atmosphere, these new peaks did not appear. If it is focused on the 1577 cm^{-1} peak, intensity value increases as potential increases (Figure 13), because a larger amount of carbon dioxide is reduced.

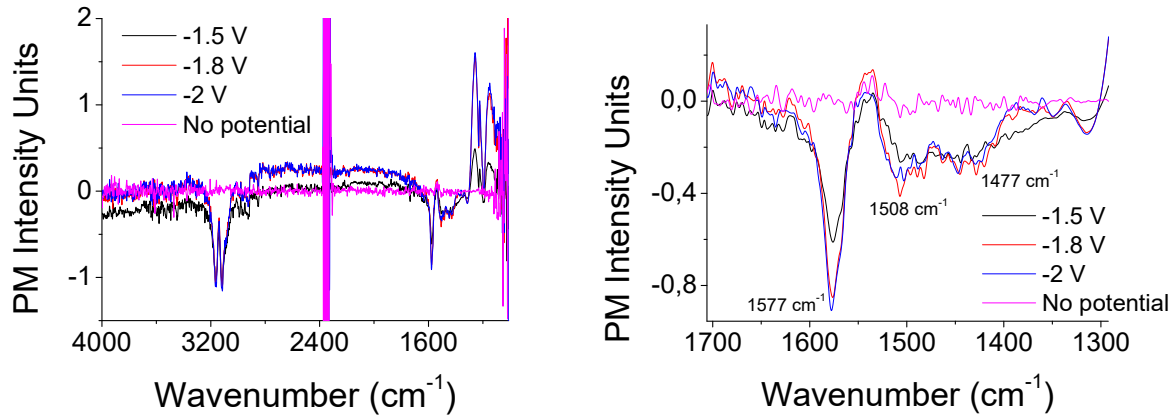

Figure 12. PM IRRAS of amperometric determinations of EMIM OTf at different applied potentials, after 1 h. After subtractions of blank, under CO_2 atmosphere. **(a)** all wavelength **(b)** zoom at determined wavelength (1300-1700 cm^{-1}).

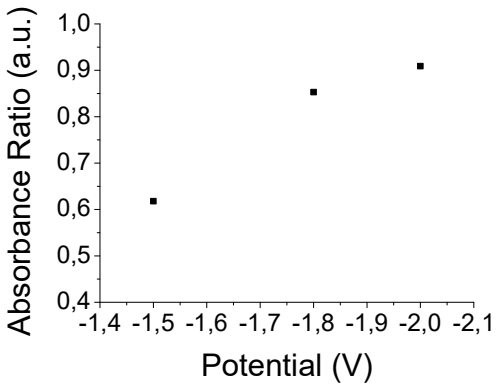

Figure 13. Absorbance ratio versus potential applied at 1577 cm^{-1} peak.

To check that the new peaks are related to CO_2 reduction products, additional experiments were conducted, wherein an applied potential of -2.0 V (vs Pt) was held on the system for 2 h, followed by a brief nitrogen purge to remove carbon dioxide. Figure 14 shows the current vs time response of the experiment, when the solution is saturated by CO_2 the current intensity value increases. However, when the CO_2 is removed from the solution, the intensity current decreases.

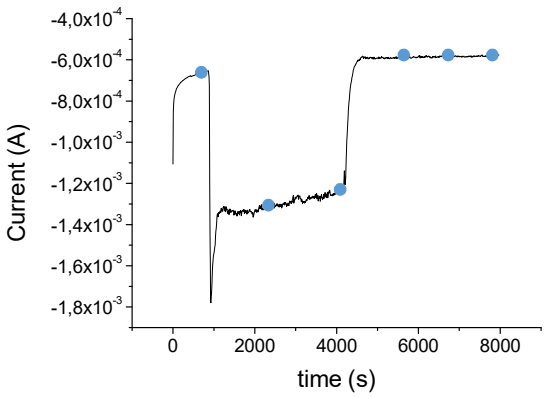

Figure 14. Current (A) versus time (s) response of amperometry experiment at -2.0 V (vs Pt). Ag WE, Pt CE, Pt QuasiRE. T= 15ºC.

With all these data, it is possible to see that CO_2 is reduced in EMIM OTf. However, the infrared measurements show no detectable amounts of CO, oxalate, or carbamate species. Instead, a carboxylated ionic liquid was produced. It is believed that when CO_2 radical anion is generated, it reacts with the ionic liquid structure after an absorption process of both reactants (Scheme 4). In this mechanism, the imidazolium ring is oriented into the surface promoting an easy attachment of the carbon dioxide reduced species to the surface. [51–56] This hypothesis is supported by the measured infrared absorption frequencies, since new peaks appear in the same region of EMIM ring functional groups. Finally, after the CO_2 radical anion forms the carboxylate with the EMIM cation, a desorption process from the electrode surface is taking place. It is important to highlight that the strong solvation effects of CO_2 radical anion in imidazolium ILs prevents the dimerization reaction avoiding the formation of oxalate, carbonate or CO and favoring the electrocarboxylation of the EMIM cation after an adsorption process.

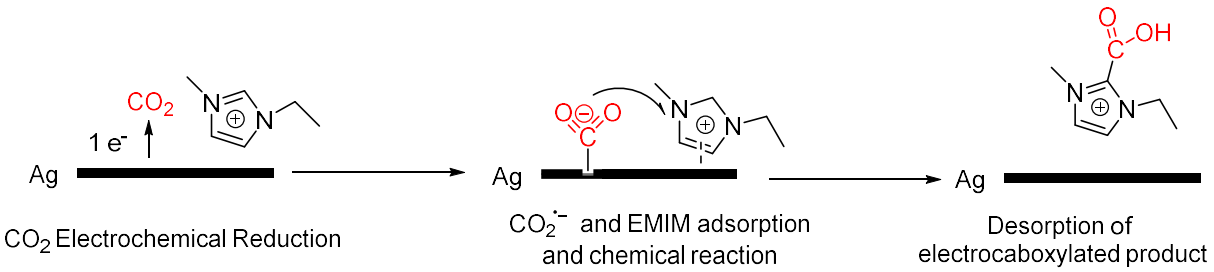

Scheme 4. Proposed carboxylation process for synthesis of EMIM OTf carboxylated ionic liquid.

4. CONCLUSIONS

The use of electrochemical, spectroscopic and molecular dynamics techniques has been revealed as a very attractive approach so as to disclose the electrochemical reduction mechanism of CO_2 depending on the electrolyte used. In this sense:

- When organic electrolytes are used the electrochemical reduction mechanism of CO_2 can be disclosed using standard electrochemical techniques such as cyclic voltammetry and controlled potential electrolysis. The use of silver and copper electrode working materials yielded to oxalate through CO_2 dimerization processes.
- The replacement of organic electrolytes for imidazolium ionic liquids allows also to switch the CO_2 reduction mechanism moving from the production of oxalate to the electrocarboxylation of the imidazolium moieties of the ILs. The solvation of CO_2 anion radical by the imidazolium cation favors the electrocarboxylation process of the ionic liquid avoiding the CO_2 dimerization process. The use of altogether of complementary techniques such as spectroelectrochemistry based on cyclic voltammetry coupled with PM IRRAS and IRRAS as well as molecular modeling simulation tools has revealed as very powerful tools to fully understand the CO_2 anion radical reactivity in ionic liquids.

ACKNOWLEDGMENTS

The authors thank the Ministerio de Ciencia e Innovación of Spain for financial support though the projects CTQ 2015-65439-R and PID2019-106171RB-I00. SM acknowledges the Autonomous University of Barcelona for her predoctoral PIF grant. SKS thanks the University of Iowa Department of Chemistry for support of this project. The invitation by the E3TECH Spanish Network of Excellence (CTQ2017-90659-REDT (MEIC/AEI)) is also kindly acknowledged. JF acknowledges CESGA supercomputing center for computer time and technical support at the Finisterrae supercomputer and financial support from MINECO Severo Ochoa programme, Grant CEX2019-000917-S. We thank Dr Piotr Kubisiak for sharing his datafiles with us.

REFERENCES

[1] T. Owen, R.D. Cess, V. Ramanathan, Enhanced CO2 greenhouse to compensate for reduced solar luminosity on early Earth, Nature. 277 (1979) 640–642. doi:10.1038/277640a0.

[2] P. Ciais, C. Sabine, G. Bala, L. Bopp, V. Brovkin, J. Canadell, A. Chhabra, R. DeFries, J. Galloway, M. Heimann, C. Jones, C. Le Quéré, R.B. Myneni, S. Piao, P. Thornton, Carbon and Other Biogeochemical Cycles, in: Intergovernmental Panel on Climate Change (Ed.), Clim. Chang. 2013 - Phys. Sci. Basis, Cambridge University Press, Cambridge, United Kingdom and New York, NY, USA, 2013: pp. 465–570. doi:10.1017/CBO9781107415324.015.

[3] J.E. Szulejko, P. Kumar, A. Deep, K.H. Kim, Global warming projections to 2100 using simple CO2greenhouse gas modeling and comments on CO2climate sensitivity factor, Atmos. Pollut. Res. 8 (2017) 136–140. doi:10.1016/j.apr.2016.08.002.

[4] A.A. Lacis, G.A. Schmidt, D. Rind, R.A. Ruedy, Atmospheric CO2: Principal control knob governing Earth's temperature, Science. 330 (2010) 356–359. doi:10.1126/science.1190653.

[5] R.S.J. Tol, The Social Cost of Carbon, Annu. Rev. Resour. Econ. 3 (2011) 419–443. doi:10.1146/annurev-resource-083110-120028.

[6] C.F. Schleussner, T.K. Lissner, E.M. Fischer, J. Wohland, M. Perrette, A. Golly, J. Rogelj, K. Childers, J. Schewe, K. Frieler, M. Mengel, W. Hare, M. Schaeffer, Differential climate impacts for policy-relevant limits to global warming: The case of 1.5 °C and 2 °C, Earth Syst. Dyn. 7 (2016) 327–351. doi:10.5194/esd-7-327-2016.

[7] M. Bui, C.S. Adjiman, A. Bardow, E.J. Anthony, A. Boston, S. Brown, P.S. Fennell, S. Fuss, A. Galindo, L.A. Hackett, J.P. Hallett, H.J. Herzog, G. Jackson, J. Kemper, S. Krevor, G.C. Maitland, M. Matuszewski, I.S. Metcalfe, C. Petit, G. Puxty, J. Reimer, D.M. Reiner, E.S. Rubin, S.A. Scott, N. Shah, B. Smit, J.P.M. Trusler, P. Webley, J. Wilcox, N. Mac Dowell, Carbon capture and storage (CCS): The way forward, Energy Environ. Sci. 11 (2018) 1062–1176. doi:10.1039/c7ee02342a.

[8] J.F.D. Tapia, J.Y. Lee, R.E.H. Ooi, D.C.Y. Foo, R.R. Tan, A review of optimization and decision-making models for the planning of CO2 capture, utilization and storage (CCUS) systems, Sustain. Prod. Consum. 13 (2018) 1–15. doi:10.1016/j.spc.2017.10.001.

[9] M. Asif, M. Suleman, I. Haq, S.A. Jamal, Post-combustion CO2 capture with chemical absorption and hybrid system: current status and challenges, Greenh. Gases Sci. Technol. 8 (2018) 998–1031. doi:10.1002/ghg.1823.

[10] M. Ramdin, T.W. De Loos, T.J.H. Vlugt, State-of-the-art of CO2 capture with ionic liquids, Ind. Eng. Chem. Res. 51 (2012) 8149–8177. doi:10.1021/ie3003705.

[11] G. De Guido, M. Compagnoni, L.A. Pellegrini, I. Rossetti, Mature versus emerging technologies for CO2 capture in power plants: Key open issues in post-combustion amine scrubbing and in chemical looping combustion, Front. Chem. Sci. Eng. 12 (2018) 315–325. doi:10.1007/s11705-017-1698-z.

[12] J. Kothandaraman, A. Goeppert, M. Czaun, G.A. Olah, G.K. Surya Prakash, CO2 capture by amines in aqueous media and its subsequent conversion to formate with reusable ruthenium and iron catalysts, Green Chem. 18 (2016) 5831–5838. doi:10.1039/c6gc01165a.

[13] F.K. Chong, V. Andiappan, D.K.S. Ng, D.C.Y. Foo, F.T. Eljack, M. Atilhan, N.G. Chemmangattuvalappil, Design of Ionic Liquid as Carbon Capture Solvent for a Bioenergy System: Integration of Bioenergy and Carbon Capture Systems, ACS Sustain. Chem. Eng. 5 (2017) 5241–5252. doi:10.1021/acssuschemeng.7b00589.

[14] M. Aghaie, N. Rezaei, S. Zendehboudi, A systematic review on CO2 capture with ionic liquids: Current status and future prospects, Renew. Sustain. Energy Rev. 96 (2018) 502–525. doi:10.1016/j.rser.2018.07.004.

[15] J.E. Bara, D.E. Camper, D.L. Gin, R.D. Noble, Room-Temperature ionic liquids and composite materials: Platform technologies for CO2 capture, Acc. Chem. Res. 43 (2010) 152–159. doi:10.1021/ar9001747.

[16] Z. Hu, Y. Wang, B.B. Shah, D. Zhao, CO2 Capture in Metal-Organic Framework Adsorbents: An Engineering Perspective, Adv. Sustain. Syst. 3 (2019) 1800080 (1–21). doi:10.1002/adsu.201800080.

[17] D.M. D'Alessandro, B. Smit, J.R. Long, Carbon dioxide capture: Prospects for new materials, Angew. Chemie - Int. Ed. 49 (2010) 6058–6082. doi:10.1002/anie.201000431.

[18] E. Torralba-Calleja, J. Skinner, D. Gutiérrez-Tauste, CO2 Capture in Ionic Liquids: A Review of Solubilities and Experimental Methods, J. Chem. 2013 (2013) 1–16. doi:10.1155/2013/473584.

[19] M. Alvarez-Guerra, J. Albo, E. Alvarez-Guerra, A. Irabien, Ionic liquids in the electrochemical valorisation of CO2, Energy Environ. Sci. 8 (2015) 2574–2599. doi:10.1039/C5EE01486G.

[20] D. Yang, Q. Zhu, B. Han, Electroreduction of CO2 in Ionic Liquid-Based Electrolytes, Innov. 1 (2020) 100016 (1–25). doi:10.1016/j.xinn.2020.100016.

[21] Y. Chen, T. Mu, Conversion of CO2 to value-added products mediated by ionic liquids, Green Chem. 21 (2019) 2544–2574. doi:10.1039/C9GC00827F.

[22] H. Senboku, A. Katayama, Electrochemical carboxylation with carbon dioxide, Curr. Opin. Green Sustain. Chem. 3 (2017) 50–54. doi:10.1016/j.cogsc.2016.10.003.

[23] E.E.L. Tanner, C. Batchelor-McAuley, R.G. Compton, Carbon dioxide reduction in room-temperature ionic liquids: The effect of the choice of electrode material, cation, and anion, J. Phys. Chem. C. 120 (2016) 26442–26447. doi:10.1021/acs.jpcc.6b10564.

[24] H. Tateno, K. Nakabayashi, T. Kashiwagi, H. Senboku, M. Atobe, Electrochemical fixation of CO2to organohalides in room-temperature ionic liquids under supercritical CO2, Electrochim. Acta. 161 (2015) 212–218. doi:10.1016/j.electacta.2015.01.072.

[25] Q. Zhu, J. Ma, X. Kang, X. Sun, H. Liu, J. Hu, Z. Liu, B. Han, Efficient Reduction of CO2 into Formic Acid on a Lead or Tin Electrode using an Ionic Liquid Catholyte Mixture, Angew. Chemie - Int. Ed. 55 (2016) 9012–9016. doi:10.1002/anie.201601974.

[26] L. Sun, G.K. Ramesha, P. V. Kamat, J.F. Brennecke, Switching the reaction course of electrochemical CO2reduction with ionic liquids, Langmuir. 30 (2014) 6302–6308. doi:10.1021/la5009076.

[27] S. Mena, G. Guirado, Electrochemical Tuning of CO2 Reactivity in Ionic Liquids Using Different Cathodes : From Oxalate to Carboxylation Products, J. C. 6 (2020) 34 (1–21). doi:10.3390/c6020034.

[28] S. Mena, I. Gallardo, G. Guirado, Electrocatalytic Processes for the Valorization of CO2 : Synthesis of Cyanobenzoic Acid Using Eco-Friendly Strategies, Catalysts. 9 (2019) 413. doi:https://doi.org/10.3390/catal9050413.

[29] D. Niu, J. Zhang, K. Zhang, T. Xue, J. Lu, Electrocatalytic carboxylation of benzyl chloride at silver cathode in ionic liquid BMIMBF4, Chinese J. Chem. 27 (2009) 1041–1044. doi:10.1002/cjoc.200990174.

[30] J.F. Fauvarque, A. Jutand, M. Francois, Nickel catalysed electrosynthesis of anti-inflammatory agents. Part I - Synthesis of aryl-2 propionic acids, under galvanostatic conditions, J. Appl. Electrochem. 18 (1988) 109–115. doi:10.1007/BF01016213.

[31] J.F. Fauvarque, A. Jutand, M. Francois, M.A. Petit, Nickel catalysed electrosynthesis of anti-inflammatory agents. Part II - Monitoring of the electrolyses by HPLC analysis. Role of the catalyst,

J. Appl. Electrochem. 18 (1988) 116–119. doi:10.1007/BF01016214.

[32] S. Mena, J. Sanchez, G. Guirado, Electrocarboxylation of 1-cholor-(4-isobutylphenyl)ethane with a silver cathode in ionic liquids : an environmentally benign and efficient way to synthesize Ibuprofen, RSC Adv. 9 (2019) 15115–15123. doi:10.1039/C9RA01781J.

[33] S. Mena, S. Santiago, I. Gallardo, G. Guirado, Sustainable and efficient electrosynthesis of naproxen using carbon dioxide and ionic liquids, Chemosphere. 245 (2020) 125557. doi:10.1016/j.chemosphere.2019.125557.

[34] A. Gennaro, A.A. Isse, M.-G. Severin, E. Vianello, I. Bhugun, J.-M. Savéant, Mechanism of the electrochemical reduction of carbon dioxide at inert electrodes in media of low proton availability, J. Chem. Soc., Faraday Trans. 92 (1996) 3963–3968. doi:10.1039/FT9969203963.

[35] M.Z. Brela, P. Kubisiak, A. Eilmes, Understanding the Structure of the Hydrogen Bond Network and Its Influence on Vibrational Spectra in a Prototypical Aprotic Ionic Liquid, J. Phys. Chem. B. 122 (2018) 9527–9537. doi:10.1021/acs.jpcb.8b05839.

[36] K. Vanommeslaeghe, E. Hatcher, C. Acharya, S. Kundu, S. Zhong, J. Shim, E. Darian, O. Guvench, P. Lopes, I. Vorobyov, A.D. MacKerell Jr., CHARMM General Force Field (CGenFF): A force field for drug-like molecules compatible with the CHARMM all-atom additive biological force fields, J. Comput. Chem. 31 (2010) 671–690. doi:10.1002/jcc.21367.CHARMM.

[37] J.C. Phillips, D.J. Hardy, J.D.C. Maia, J.E. Stone, J. V. Ribeiro, R.C. Bernardi, R. Buch, G. Fiorin, J. Hénin, W. Jiang, R. McGreevy, M.C.R. Melo, B.K. Radak, R.D. Skeel, A. Singharoy, Y. Wang, B. Roux, A. Aksimentiev, Z. Luthey-Schulten, L. V. Kalé, K. Schulten, C. Chipot, E. Tajkhorshid, Scalable molecular dynamics on CPU and GPU architectures with NAMD, J. Chem. Phys. 153 (2020) 044130. doi:10.1063/5.0014475.

[38] W. Humphrey, A. Dalke, K. Schulten, VMD: Visual Molecular Dynamics, J. Mol. Graph. 14 (1996) 33–38.

[39] A. J. Bard, L. A. Faulkner, Fundamentals and Applications, 2nd ed., Austin, 1990.

[40] A. J. Bard, L.R. Faulkner, Electrochemical methods: Fundamentals and applications, 2nd ed., John Wiley & Sons, Inc., New York, 2001. doi:10.1038/s41929-019-0277-8.

[41] I. Reche, I. Gallardo, G. Guirado, Cyclic voltammetry using silver as cathode material: A simple method for determining electro and chemical features and solubility values of CO2 in ionic liquids, Phys. Chem. Chem. Phys. 17 (2015) 2339–2343. doi:10.1039/c4cp05409a.

[42] L. Zhang, Y.-W. Luo, D.-F. Niu, L.-P. Xiao, J.-X. Lu, Electrochemical Behavior of CO2 on Copper Electrode, Chem. J. Chinese Univ. 28 (2007) 1660–1662.

[43] R.G. Compton, C.E. Banks, Understanding Voltammetry, World Scientific (Europe), 2018. doi:10.1142/q0155.

[44] Y. Gholami, R. Azin, R. Fatehi, S. Osfouri, Suggesting a numerical pressure-decay method for determining CO2 diffusion coefficient in water, J. Mol. Liq. 211 (2015) 31–39. doi:10.1016/j.molliq.2015.06.060.

[45] B. Jähne, G. Heinz, W. Dietrich, Measurement of the diffusion coefficients of sparingly soluble gases in water, J. Geophys. Res. Ocean. 92 (1987) 10767–10776. doi:10.1029/JC092iC10p10767.

[46] T.J.H. Vlugt, J.P.J.M. van der Eerden, M. Dijkstra, S. Berend, D. Frenkel, Introduction to Molecular Simulation and Statistical Thermodynamics, Delft, 2009. http://homepage.tudelft.nl/v9k6y/imsst/.

[47] M. Shamsipur, A.A.M. Beigi, M. Teymouri, S.M. Pourmortazavi, M. Irandoust, Physical and electrochemical properties of ionic liquids 1-ethyl-3-methylimidazolium tetrafluoroborate, 1-butyl-3-methylimidazolium trifluoromethanesulfonate and 1-butyl-1-methylpyrrolidinium bis(trifluoromethylsulfonyl)imide, J. Mol. Liq. 157 (2010) 43–50. doi:10.1016/j.molliq.2010.08.005.

[48] A. Hailu, S.K. Shaw, Efficient Electrocatalytic Reduction of Carbon Dioxide in 1-Ethyl-3-methylimidazolium Trifluoromethanesulfonate and Water Mixtures, Energy and Fuels. 32 (2018) 12695–12702. doi:10.1021/acs.energyfuels.8b02750.

[49] A.M. Cione, O.A. Mazyar, B.D. Booth, C. McCabe, G.K. Jennings, Deposition and Wettability of [bmim][triflate] on Self-Assembled Monolayers, J. Phys. Chem. C. 113 (2009) 2384–2392. doi:10.1021/jp808098w.

[50] R.S. Anaredy, S.K. Shaw, Developing Distinct Chemical Environments in Ionic Liquid Films, J. Phys. Chem. C. 122 (2018) 19731–19737. doi:10.1021/acs.jpcc.8b06608.

[51] D.J. Faggion, W.D.G. Gonçalves, J. Dupont, CO2 Electroreduction in Ionic Liquids, Front. Chem. 7 (2019) 1–8. doi:10.3389/fchem.2019.00102.

[52] G.P.S. Lau, M. Schreier, D. Vasilyev, R. Scopelliti, M. Gra, P.J. Dyson, New Insights Into the Role of Imidazolium-Based Promoters for the Electroreduction of CO2 on a Silver Electrode, J. Am. Chem. Soc. 138 (2016) 7820–7823. doi:10.1021/jacs.6b03366.

[53] H.K. Lim, H. Kim, The mechanism of room-Temperature ionic-liquid-based electrochemical CO2 reduction: A Review, Molecules. 22 (2017) 536 (1–16). doi:10.3390/molecules22040536.

[54] K. Mei, X. He, K. Chen, X. Zhou, H. Li, C. Wang, Highly E ffi cient CO2 Capture by Imidazolium Ionic Liquids through a Reduction in the Formation of the Carbene − CO2 Complex, Ind. Eng. Chem. Res. 56 (2017) 8066–8072. doi:10.1021/acs.iecr.7b01001.

[55] B.A. Rosen, A. Salehi-Khojin, M.R. Thorson, W. Zhu, D.T. Whipple, P.J.A. Kenis, R.I. Masel, Ionic liquid-mediated selective conversion of CO2 to CO at low overpotentials, Science. 334 (2011) 643–644. doi:10.1126/science.1209786.

[56] L. Sun, G.K. Ramesha, P. V Kamat, J.F. Brennecke, Switching the Reaction Course of Electrochemical CO2 Reduction with Ionic Liquids, Langmuir. 30 (2014) 6302–6308. doi:10.1021/la5009076.